Current Research in Green and Sustainable Chemistry 5 (2022) 100236

Contents lists available at ScienceDirect

Current Research in Green and Sustainable Chemistry

journal homepage: www.elsevier.com/journals/current-research-in-green-and-sustainable-chemistry/2666-0865

Ball milling – A green and sustainable technique for the preparation of titanium based materials from ilmenite

Charitha Thambiliyagodage [a,*], Ramanee Wijesekera [b]

[a] Faculty of Humanities and Sciences, Sri Lanka Institute of Information Technology, New Kandy Road, Malabe, Sri Lanka
[b] Department of Chemistry, University of Colombo, Sri Lanka

ARTICLE INFO

Keywords:
Ball milling
Acid
Leaching
Hydrothermal
Titania

ABSTRACT

Ilmenite is a naturally available mineral that is highly applicable in the synthesis of pure TiO_2. Titania mainly presents in four polymorphs as rutile, anatase, brookite and TiO_2–B. Titania could be mined from minerals such as ilmenite, leucoxene and rutile among which ilmenite is the main source. Ball milling is a mechanical activation method used before subjecting ilmenite to chemical treatment methods to produce titanium based materials. Effect of milling time, milling intensity, milling atmosphere, the introduction of reducing agents on the particle size, surface area, annealing temperature, and the crystal structure of the products are reviewed. The effect of ball milling on acid digestion of ilmenite in hydrochloric acid and sulfuric acid is discussed. Further, the effect of mechanical activation on hydrothermal treatment of ilmenite is explained in detail.

1. Introduction

Ball milling is a mechanical technique used to grind powders into fine particles [1]. Generally, a ball mill consists of a hollow cylindrical vessel that rotates around its axis and balls which are made of materials such as steel, stainless steel, ceramic or rubber. The powder is processed by the interactions with the balls, and the friction of the balls with each other and with the wall of the vessel (Fig. 1). The milling process depends on the energy released from the collision of balls and the powder, and fine particles are produced. The ball milling method is classified as vibration mill, planetary mill and magneto-ball mill depending on the movement of the balls and vessel and among them, the planetary mill is the most common as it has been used to reduce the particle size of many materials. The ball milling process induces a reduction in the particle and crystallite size mainly. Further, it creates deformations in the crystal structure, metastable phases, surface modifications. At the initial stage of milling, powder particles are flattened by the compressive forces caused by the impact of the balls leading to changes in the shape of the particles. Fracturing and cold welding occur when powder and clusters colloid further with balls with high kinetic energy. With further milling, more refinement and reduction in the particle size is more evident and the microstructure of the particle becomes more homogeneous. After the milling process, an extremely deformed metastable structure results where the lamella are no longer resolvable by optical microscopy. Moreover, milling can trigger chemical reactions that are not favourable at room temperature. The milling process strongly depends on different parameters such as volume of the vessel, ball size, density of the balls, total ball mass, hardness of the balls, powder amount, rotational speed, feed time, milling time and the milling atmosphere. These parameters have been varied to produce fine particles from the powder/clusters and the surface area, particle size, crystal nature etc, changed depending on the conditions supplied [2–6]. Ball milling is an eco-friendly, cost-effective, reliable, reproducible technique that could be applied to different materials under dry and wet conditions. This technique possesses many advantages including cost-effectiveness, ease of operation, reliability, reproducibility, production of a fine powder, suitability for milling toxic materials since it is performed in a close vessel, appropriateness for continuous processes, applicability in wet and dry conditions on a wide range of materials etc. However, disadvantages such as the possibility of contamination, production of irregular shaped and different sized materials, long milling and cleaning time, noise etc. are associated with this technique [7]. Ball milling could be applied to various materials such as cellulose, hydroxyapatite, ilmenite, metal oxides, polymers, etc. In this paper, we reviewed the application of milling to ilmenite, the main source of TiO_2.

Ilmenite is a naturally available mineral found in igneous rocks, sediments, sedimentary rocks in many countries including Australia, South Africa, India, Brazil, Norway, Ukraine, Sri Lanka etc as shown in

* Corresponding author.
E-mail address: charitha.t@sliit.lk (C. Thambiliyagodage).

https://doi.org/10.1016/j.crgsc.2021.100236
Received 8 August 2021; Received in revised form 18 November 2021; Accepted 4 December 2021
Available online 5 December 2021

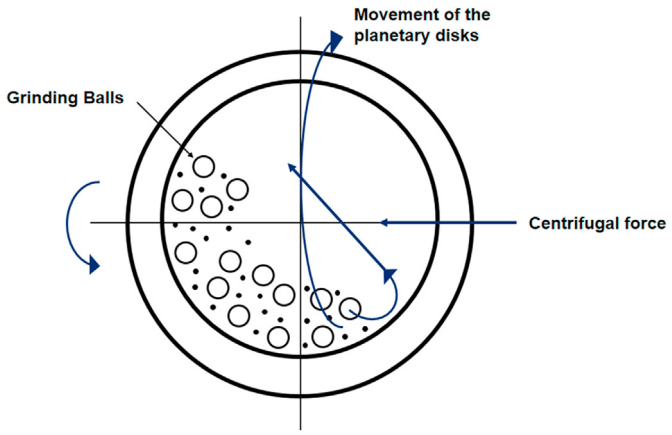

Fig. 1. Horizontal section of a grinding vessel and powder mixture.

Fig. 2. The composition of ilmenite varies from one location to the other and generally, ilmenite consists of TiO_2, FeO, Fe_2O_3, Na_2O, SiO_2, Al_2O_3, ZrO_2, Cr_2O_3, MnO, CaO, MgO, SnO_2, K_2O, V_2O_5, P_2O_5, SO_3 as revealed by XRF analysis performed [9–12]. Ilmenite is known as the raw material to synthesize white pigment TiO_2 [9,13,14]. Ilmenite is subjected to many treatment conditions especially digestion in acids like hydrochloric and sulfuric acids, to synthesize pure TiO_2 or to extract its constituent elements (Ti and Fe) used for different applications. TiO_2 is well known in the world for its applicability in different applications including but not limited to photocatalysis to produce H_2 [15–17] and to degrade organic pollutants such as textile dyes [18–20], pharmaceuticals [21–23], and pesticides [24,25], in photovoltaic cells [26,27], as the anode material in Lithium-ion batteries [28,29], as a white pigment in paints, coatings, plastics [30] etc. In view of the vast potential that TiO_2 has, it is important to explore other sources of TiO_2 as an alternative to the expensive process of synthesizing it. With such wide applicability of TiO_2, researchers came across different synthesis methods to synthesize TiO_2 using different chemical precursors. Electrophoretic deposition [31], spray pyrolysis [32], sonochemical [33] and microwave-assisted methods [34], hydro/solvothermal methods [34]and sol-gel methods [35] are used to synthesize Ti based materials. Those methods use precursors including Titanium isopropoxide [36], titanium butoxide [37], titanium oxyacetylacetonate [38], titanium tetrachloride [39] which are expensive. Therefore, it is of great importance to use a naturally available material, as discussed in this review ilmenite as the starting material to synthesize TiO_2 and titanium based materials. There are many methods available such as acid leaching [9,40–43], hydrothermal synthesis [44,45] leaching in alkalines [46,47] etc.

Reviews are available on acid leaching of ilmenite [48–50] but to our knowledge, a review on mechanical activation applied along with the other treatment techniques is not available. Ball milling is used as a preliminary technique performed before main techniques. Mechanical activation by ball milling is known to increase the reactivity of the material and the uniformity of spatial distribution of elements [51,52]. During mechanical activation potential energy of the materials are enhanced and such increased energy is expressed as an increase in surface area, vacancy and dislocation concentrations, enhancement in metastable phases, structural disorder, alteration in bond length/angles,

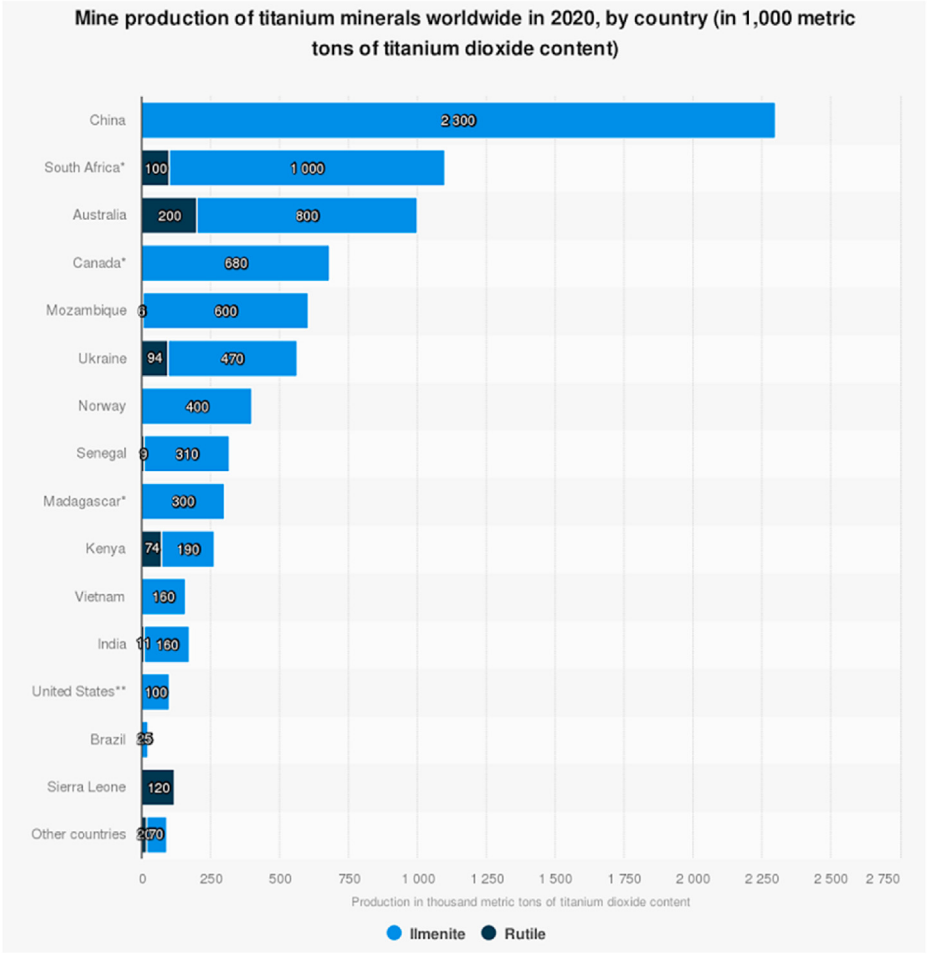

Fig. 2. Worldwide mine production of titanium minerals in 2020. Adapted from Ref. [8].

higher oxidation states etc [53,54]. Such created changes enhance the activities followed by mechanical activation. In this review, we discuss the process of mechanical activation of ilmenite and its enhanced contribution to acid leaching of ilmenite and hydrothermal synthesis of Ti-based materials from ilmenite.

2. Ball milling

2.1. Activated carbon as the reducing agent

The ball milling technique has been widely used to synthesize TiO_2 nanomaterials via top down approach. Y. Chen et al. [55,56] have studied the ball milling of Australian ilmenite under a variety of conditions. Ilmenite was mixed with granular activated carbon in a weight ratio of 4:1 to ensure the complete carbothermic reduction of ilmenite. Ilmenite ball milled at room temperature reduced to rutile, iron and austenite at the low annealing temperature. As shown the Fig. 3 (i) the first weight loss was observed in the temperature range 100 °C–850 °C, the second dramatic decrease was above 850 °C with a total weight loss of 21.5 wt%, whereas in the carbon-ilmenite mixture which was not subjected to milling a significant weight loss was observed over 800 °C. The thermogravimetric curve of the premilled sample clearly shows three regions as (a), (b) and (c) where region (a) corresponds to the low-temperature solid-state reduction that typically occurs from 860 °C to 1000 °C given by,

$$FeTiO_3(S) + C(S) = Fe(S) + TiO_2(S) + CO(g)$$

Region (b) corresponds to the high-temperature reduction of ilmenite by gaseous CO usually above 1000 °C.

$$FeTiO_3(S) + CO(g) = TiO_2(S) + Fe(s) + CO_2(g)$$

With CO generation,

$$C(S) + CO_2(g) = 2\ CO(g)$$

Typically above 1200 °C further reduction of rutile occurs,

$$TiO_2(s) + CO(g) = Ti_3O_5(s) + CO_2(g)$$

According to the XRD patterns at an annealing temperature of 760 °C, some of the ilmenite was reduced to TiO_2, producing some α-Fe and Fe(C) phases. On increasing the annealing temperature to 900 °C, rutile was the dominant phase. With the increase in the annealing temperature to 1100 °C, a new reduction product appeared as γ-Ti_3O_5 together with α-Fe and Fe(C), indicating a further reduction of rutile and complete disappearance of ilmenite. Moreover, high milling time also led to a decrease in the annealing temperature for conversion of ilmenite to rutile. The ilmenite and carbon mixture milled for different durations (100, 200 and 400 hours) showed interesting results. The onset temperatures of the second stage where rutile appeared to be the dominant phase, for samples milled at 100, 200 and 400 hours were 900 °C, 850 °C and 750 °C, respectively (Fig. 3 (ii)) and the weight loss after heating at 1100 °C was 17.5, 21.5, 24 wt%, respectively. Further, with high milling intensity, the reduction temperature also decreased showing a weight loss of 24.5 wt%, and a weight loss of 22.1 wt% resulted in low milling intensity. Authors indicate that O_2 should be absent in the milling process because the presence of O_2 leads to different solid-state reactions, and atmospheres such as vacuum, Ar, and N_2 are suggested as alternatives [55]. Chen et al. [57] further studied the effect of milling atmosphere on the chemical nature of the resulting material after milling. Ilmenite which was subjected to ball milling under vacuum does not change its chemical nature. However, ilmenite milled in air showed the presence of $Fe_2Ti_3O_9$ after 100/200 hours of milling an observation consistent with that of Grey and Reid

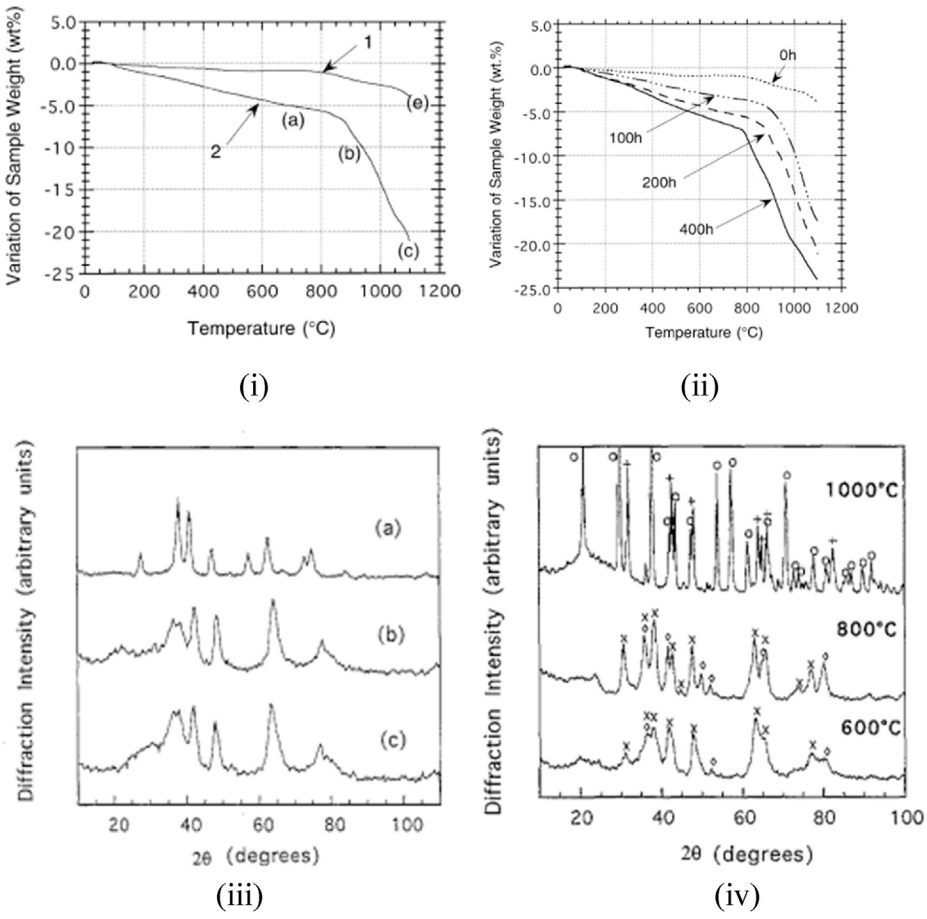

Fig. 3. TG curves of ilmenite-carbon mixture (i) 1. without premilling 2. With premilling at intensity 2 for 200 hours, annealed at (a) 760 °C, (b) 900 °C and (c) and (e) 1100 °C (ii) milled for different durations at an intensity of 2. Adapted from Ref. [55]. (iii) XRD patterns of the ilmenite samples after milling at different milling conditions (a) 200 hours under vacuum (b) 100 h in air (c) 200 h in air. (iv) XRD patterns of premilled ilmenite samples in air, annealed at different temperatures. X: $Fe_2Ti_3O_9$, ⋄: Fe_2O_3, +: TiO_2, O: Fe_2TiO_5. Adapted from Ref. [57].

[58]. Fig. 3 (iii) and (iv) show XRD patterns of the samples after milling (200 hours) and annealing in a differential thermal analyzer (600 °C, 800 °C and 1000 °C). Samples annealed at 600 °C showed only the diffraction peaks of $Fe_2Ti_3O_9$ while that annealed at 800 °C showed $Fe_2Ti_3O_9$ as the dominant phase and diffraction peaks attributed to maghemite (γ-Fe_2O_3). This new product of oxidation was not detected in the sample milled in air at room temperature probably due to the small grain size and/or the disordered structure. After annealing at 1000 °C only the TiO_2 and Fe_2TiO_5 were detected. This indicated that the formed $Fe_2Ti_3O_9$ decomposed to TiO_2 and Fe_2TiO_5 at 1000 °C and γ-Fe_2O_3 probably reacted with TiO_2 to produce Fe_2TiO_5 [59]. All the chemical reactions for premilled ilmenite are given below.

At temperatures below 800 °C only part of the ilmenite oxidizes,

$$6\ FeTiO_3(S) + 3/2\ O_2(g) = 2\ Fe_2Ti_3O_9(S) + Fe_2O_3(S)$$

At temperatures greater than 800 °C, two reactions could happened,

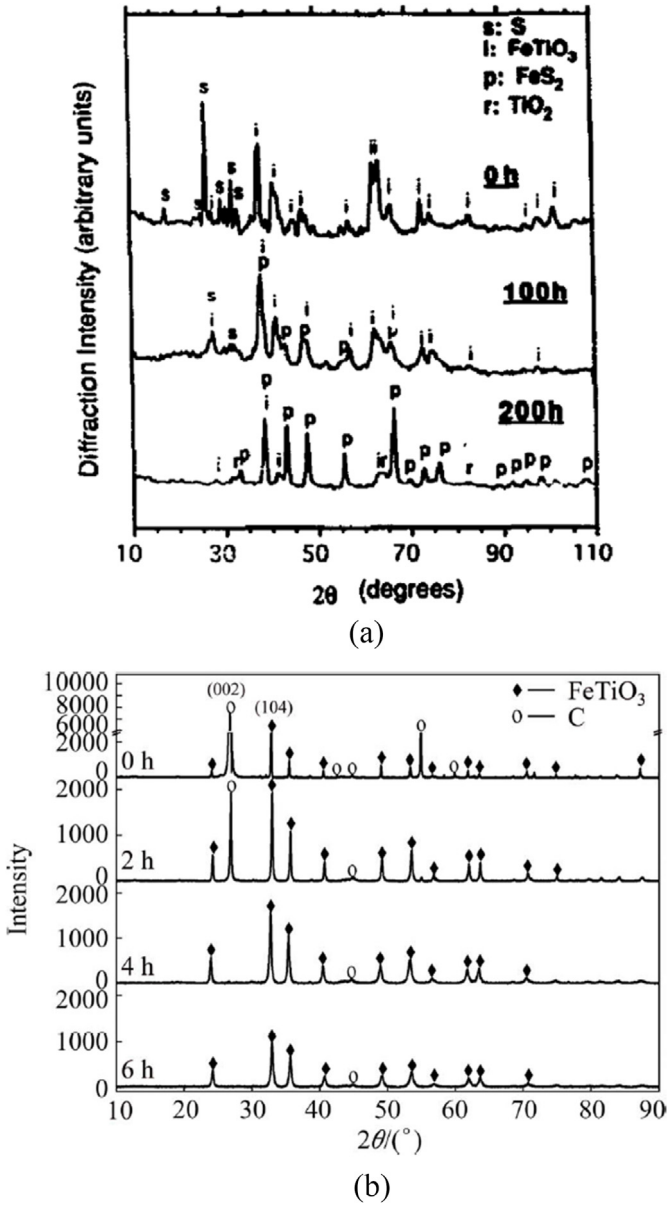

Fig. 4. (a) XRD patterns recorded from the mixtures of ilmenite and sulfur milled for different periods. Adapted from Ref. [61]. (b) XRD patterns of milled and unmilled samples. Adapted from Ref. [62].

$$4\ FeTiO_3(S) + O_2(g) = 2\ Fe_2TiO_5(S) + 2TiO_2(S)$$

$$Fe_2Ti_3O_9(S) = Fe_2TiO_5(S) + 2TiO_2(S)$$

Interestingly, ilmenite which was not premilled before annealing showed ilmenite as the dominant phase with TiO_2 and $Fe_2Ti_3O_9$ in small quantities after annealing at 600 °C. The quantity of TiO_2 and $Fe_2Ti_3O_9$ increased in the sample annealed at 800 °C. Though the major phase was still ilmenite, minor quantities of α- Fe_2O_3 were detected. Similarly, to the premilled sample, at 1000 °C only TiO_2 and Fe_2TiO_5 were detected. Chemical reactions that occur during annealing of ilmenite without premilling are as follows,

At temperatures lower than 800 °C,

$$4\ FeTiO_3(S) + O_2(g) = Fe_2Ti_3O_9(S) + Fe_2O_3(S) + TiO_2(S)$$

At temperatures greater than 800 °C,

$$4\ FeTiO_3(S) + O_2(g) = 2\ Fe_2TiO_5(S) + 2\ TiO_2(S)$$

Hence, the authors concluded that the process of oxidation of ilmenite induced by high energy ball milling is a non-equilibrium process and is favourable for the formation of metastable phases [57]. Further, it was found that ilmenite fully oxidized to Fe_2TiO_5 and TiO_2 by heating to 1000 °C in air, could be converted to $Fe_2Ti_3O_9$ by ball milling in oxygen gas, which is also the product formed on milling ilmenite in air at room temperature without annealing [60].

$$Fe_2TiO_5(S) + TiO_2(S) = Fe_2Ti_3O_9(S)$$

2.2. Sulfur as the reducing agent

Ball milling of the ilmenite-sulfur mixture at room temperature in a vacuum was also investigated [61]. Upon ball milling broadening of the diffraction peaks in the XRD pattern (Fig. 4 (a)) corresponding to ilmenite was observed due to the reduction in crystallite size of ilmenite induced by ball pulverization. In addition, peaks corresponding to FeS_2, which became more prominent with increasing milling time, could also be seen. Weak peaks of TiO_2 were also present. However, when a premilled ilmenite sulfur mixture was annealed under Ar flow, the sample annealed at 400 °C showed prominent peaks for FeS_2 and low-intensity peaks for TiO_2. The sample annealed at 600 °C resulted in the production of TiO_2 in larger amounts and disappearance of the FeS_2 phase and the formation of Fe_9S_{10}. Interestingly, the sample annealed at 800 °C showed the presence of only TiO_2. Pure rutile powder was obtained by acid leaching the sample annealed at 600 °C in 10% HCl and Fe_9S_{10} was leached suggesting that this low-temperature extraction process is a simple and low-cost alternative for producing rutile from ilmenite [61].

2.3. Graphite as the reducing agent

Structural changes of ilmenite ball milled with graphite under Ar atmosphere were studied [62]. X-ray diffraction patterns (Fig. 4 (b)) showed that the intensity of the characteristic diffraction peak of graphite (002) decreased by 95% after 2 hours of milling and completely disappeared after 4 hours indicating that the graphite crystalline structure easily deformed along the (002) crystal plane to produce amorphous carbon. A reduction in the intensity of the ilmenite (104) peak was also observed due to the reduction in particle size during the milling process. The authors studied the behaviour of the premilled ilmenite graphite mixture heated to 1400 °C under flowing N_2. It could be been seen that the TG curve of the unmilled sample has not reached a steady level with an increase in temperature to 1400 °C (Fig. 5). A weight loss was observed during the solid-state reduction of ilmenite with carbon on milling for more than 4 hours. Fe and TiO_2 were the solid products while the gaseous product was CO. According to the DSC study (Fig. 5),

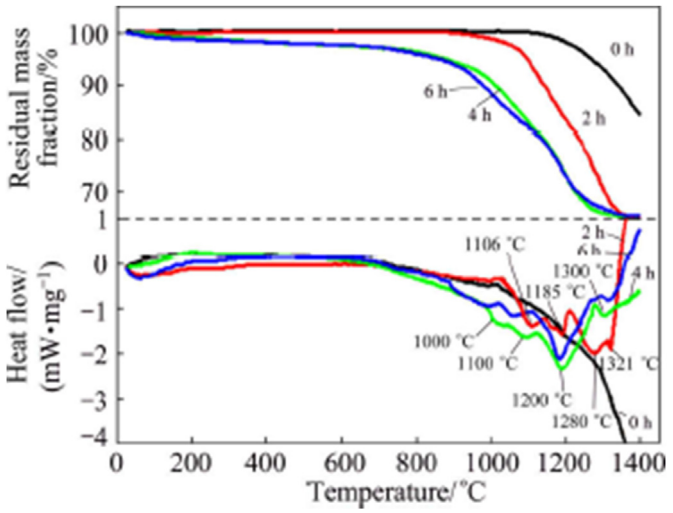

Fig. 5. TG and DSC curves of unmilled and milled samples as a function of temperature. Adapted from Ref. [62].

endothermic peaks that stand for gradual deoxidizing of titanium oxides could be seen at different temperatures in samples milled for 2 hours (1106, 1185, 1280, 1321 °C) and 4 hours (1000, 1100, 1200, 1300 °C). The first two endothermic peaks were assigned to the formation of Ti_4O_7 and Ti_3O_5 as follows,

$$TiO_2(S) + 1/4C(S) = 1/4\ Ti_4O_7(S) + 1/4\ CO(g)$$

$$Ti_4O_7(S) + 1/3C(S) = 4/3\ Ti_3O_5(S) + 1/3\ CO(g)$$

The transformations of Ti_3O_5 to TiN and then to Ti(C, N) were easier under the N_2 atmosphere. The reactions corresponding to the third and fourth curves are,

$$Ti_3O_5(S) + 5C(S) + 3/2\ N_2(g) = 3\ TiN(S) + 5\ CO(g)$$

$$TiN(S) + C(S) = Ti(C,N)(S) + N_2(g)$$

The appearance of the above phases was also confirmed by XRD patterns [62]. Table 1 summarizes the parameters varied during the synthesis of different products by ball milling of ilmenite.

3. Ball milling and acid treatment

3.1. Treatment in hydrochloric acid

Tao et al. [63] reported the preparation of TiO_2 nanorods by natural ilmenite via a two-step process, involving ball milling and wet chemistry. As the first step, ball milling of ilmenite was carried out under an Ar atmosphere at room temperature for 150 hours in a ball mill consisting of a horizontal rotating stainless steel cell with four hardened steel balls. The chemical composition of ilmenite has been expressed as TiO_2 (dry bass) 49.6%, iron (total) 35.1%, FeO 32.8%, Fe_2O_3 13.7%, Al_2O_3 0.47%, Cr_2O_3 0.25%, and SiO_2 0.45%. SiO_2 impurities had been removed by treating milled ilmenite with 2 M NaOH for 2 hours at 120 °C followed by treatment with 4 M HCl at 90 °C for 4 hours. The growth mechanism of rutile nanorod has been explained as follows. Ilmenite dissolves in HCl to form $TiOCl_2$ and $FeCl_2$. Then $TiOCl_2$ hydrolyzes and precipitates as TiO_2 crystals that continue their growth in a 1D fashion as given in the following equations.

$$FeO{\cdot}TiO_2(S) + 4\ HCl(aq) = FeCl_2(aq) + TiOCl_2(aq) + 2H_2O(l)$$

$$TiOCl_{2(}aq) + H_2O(l) = TiO_2(S) + 2\ HCl(aq)$$

The rutile nanorods produced were typically 50–100 nm length 20 nm width and 2–3 nm thick. They absorb light of wavelengths 400–450 nm, different to that of commercial P25 TiO_2 nanoparticles which do not exhibit absorption beyond 350 nm. This has been attributed to the presence of iron as an impurity in small quantities. When TiO_2 nanorods were used as anode material for lithium-ion batteries they showed remarkable rate capability, high reverse capacity and good cycling stability. Further, these nanorods have been effective photocatalysts in mineralizing oxalic acid under near UV illumination. Their activity is higher than that of P25 TiO_2 due to the small quantities of the iron present which enhance the photocatalytic activity [63]. The preparation of TiO_2 from natural ilmenite via four steps: Ball milling with activated carbon, annealing, leaching by acid and finally calcining in the air is also reported [64]. Ilmenite was mixed with activated carbon in a weight ratio of 4:1 and was milled as described above. The milled mixture was then annealed at 1000 °C for 60 minutes. The annealed sample was treated with 4 M HCl at 90 °C for 4 hours. After leaching, the sample was filtered, and the leached sample was washed and dried at 90 °C for 4 hours. The acid leached sample was then calcined in air at 600 °C for 2 hours to remove the residual activated carbon [64]. Ball milling reduces the carbothermal reduction temperature [56]. The effects of pretreating ilmenite by ball milling have been attributed to the creation of crystal defects and lattice distortions, decrease in particle size and increase in the surface area [55,65]. X-ray diffraction patterns (Fig. 6 (i)) of the milled mixture annealed at different durations (0.5, 1 and 1.5 hours), clearly showed that the ilmenite predominant XRD pattern with weak peaks for rutile and Fe(C) (austenite) on annealing for 0.5 hours, converted to a rutile rich sample high in Fe(C) (austenite) and low in iron (Fe) on annealing for 1 hour. However, with prolonged annealing time, the rutile phase predominated while the peaks for Fe(C) (austenite) decreased in intensity and the intensity of the peak for iron (Fe) increased dramatically indicating the conversion of Fe(C) (austenite) to iron (Fe) (Fig. 6 (i) b and C). Bimodal pore size distribution was reported during this synthesis. When the samples were annealed for 0.5 hours the pore size distribution curve showed two peaks; one ranging from 5 to 40 nm with a maximum at about 10–15 nm indicating the presence of small mesopores while the less dominant peak centered around 70 nm showed the presence of larger pores. Pores of the samples annealed for 1.5 hours were dominated by pores in the range of 40–90 nm, while the sample annealed for 1 hour showed two peaks indicating the bimodal pore distribution (Fig. 6 (ii)). In general, acid leaching removed iron and other impurities (Ca^{2+}, Mg^{2+} etc.) producing high grade titanium dioxide. Further, the development of small pores within the nanoparticles is caused by the acid leaching of iron directly from ilmenite. Larger pores are the spaces between nanoparticle aggregates. The acid leached sample was calcined in air to remove the carbon added at the ball milling. The surface area and the total pore volume of the acid leached sample were higher than those of the milled mixture. However, the above parameters were found to be lower in the calcined sample than those in the acid leached sample due to the reduction in carbon content and sintering of TiO_2 particles. The produced TiO_2 material with bimodal pore distribution was found to be more effective in photodegradation of phenol than the commercial TiO_2 because porous TiO_2 is reported to possess an increased light absorption as well as high surface area. Moreover, the onset wavelength of the band gap absorption of the prepared porous TiO_2 is 458 nm compared to commercial TiO_2 in which it is 360 nm. This has been attributed to the defects created and impurities such as iron and carbon introduced, making TiO_2 effective in the visible region as well [64]. A composite of TiO_2 and carbon prepared similarly except for the calcination step was found to exhibit effective electrochemical performance as anodes in lithium-ion batteries due to the synergistic effect of TiO_2 and carbon [66].

Leaching of ilmenite found in Panxi-China in 20 wt% HCl with and without mechanical activation was studied with the objective of leaching mainly iron, magnesium, and calcium from ilmenite. Congruency of extraction is a parameter used to determine the uniform incorporation of two metals in the structure of a mineral. It has been found that magnesium uniformly occupies the iron sites throughout ilmenite as it exhibited

Table 1
Parameters of producing different products by ilmenite *via* ball milling.

Reducing agent	Ilmenite: reducing agent weight ratio	Temperature	Milling Intensity/ Milling Speed	Duration (h)	Atmosphere	Particle size before milling	The particle size after ball milling	Surface area	Annealing Temperature after milling (°C)	Products after annealing		Reference
										Dominant Phase	Other phases	
Granular activated carbon	4 : 1	Room temperature	20 steel balls (Diameter – 8.6 mm)	400	Vacuum	300 μm	50 nm	12.0	–	-	–	[55]
			4 steel balls (Diameter – 25.4 mm)	100				14.1	–	–	–	
				200				–	760	$FeTiO_3$	TiO_2, α-Fe, γ-Fe(C)	
									900	TiO_2, α-Fe, γ-Fe(C)	$FeTiO_3$	
									1100	γ-Ti_3O_9, α-Fe, γ-Fe(C)	–	
				400				–	–	–	–	
			5 steel balls (Diameter – 25.4 mm)	200				15.4	–	–	–	
–	–	Room Temperature	5 steel balls (Diameter – 25.4 mm)	200	air	200–300 μm			600	$Fe_2Ti_3O_9$	-	[57]
									800	$Fe_2Ti_3O_9$	γ-Fe_2O_3	
									1000	TiO_2, Fe_2TiO_5	–	
Sulfur	6:2.5	Room Temperature	5 steel balls (Diameter – 25.4 mm)	100	Vacuum	200–300 μm	–	–	400	FeS_2	$FeTiO_3$, TiO_2	[61]
									600	TiO_2, Fe_9S_{10}	–	
				200					400	FeS_2	TiO_2	
									600	Fe_9S_{10} TiO_2	–	
									800	Fe_9S_{10} >TiO_2	–	
Graphite	–	–	250 r/min 350 r/min 450 r/min	4	Ar	~ 160 μm	–	–	1000	Fe	$FeTiO_3$, TiO_2, C	[62]
									1100	Fe	Ti_4O_7, C	
									1200	Ti_3O_5, TiN	Fe, C, Fe_3C	
									1300	Fe, Ti(C,N)	Ti_3O_5	
									1400	Fe, Ti(C,N)	–	

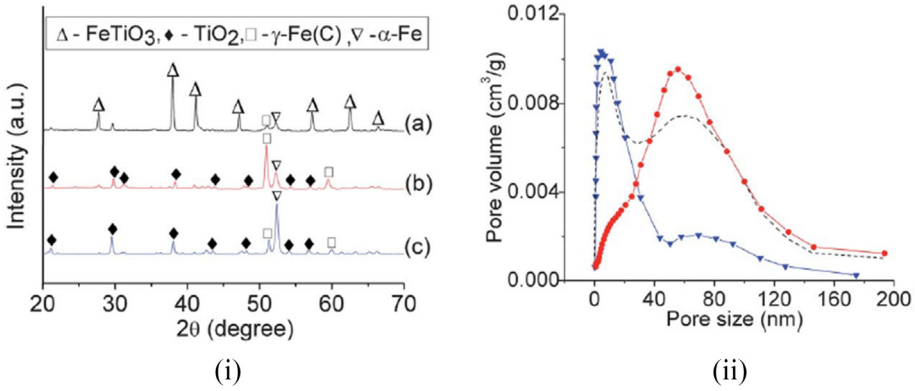

Fig. 6. (i) XRD patterns of ilmenite carbon mixture annealed at 1000 °C for (a) 0.5 h (b) 1 h (c) 1.5 h. (ii) Pore size distribution curves of the porous samples obtained after annealing for different lengths of time, 0.5 h (▼) or 1.5 h (●), after subsequent leaching and calcining. The distribution of the sample annealed for 1 h, then leached and calcined is also shown for comparative purposes (a dashed line). Adapted from Ref. [64].

congruent extraction, while calcium incongruent extraction resulted in showing that it is heterogeneously distributed in ilmenite mostly close to or absorbed to the surface of ilmenite, causing easy dissolution in HCl. This has been supported by the EDX results where magnesium isomorphously displaced iron in the ilmenite structure while a minor amount coexisted with silicon and aluminium in gangue minerals. Areas rich in calcium are also rich in silicon suggesting that calcium is associated with gangue minerals and not with ilmenite. There were no significant differences in element distribution upon mechanical activation while prolonged mechanical activation caused more leaching of iron and magnesium than in the unmilled ilmenite. Mechanically activated ilmenite showed efficient dissolution of calcium. However, with prolonged leaching time the dissolution of calcium in both milled and unmilled ilmenite is the same, as calcium was found close to the surface of ilmenite. Therefore, acid leaching has removed metal ions from ilmenite and mechanical activation has triggered metal dissolution [67]. Similar studies have shown the effect of mechanical activation on the dissolution of ilmenite [68–71].

3.2. Treatment in sulfuric acid

High-energy ball milling was found to enhance the dissolution of ilmenite in sulfuric acid [72]. Ilmenite was ball milled in both vacuum and air; a 54% dissolution was achieved for ilmenite milled for 10 hours in a vacuum and a 98% dissolution resulted from the ilmenite sample milled for 200 hours. However, ilmenite milled in air for 10 hours produced a 51% dissolution and a 69% dissolution after 200 hours of milling as indicated by the presence of unreacted ilmenite in the XRD patterns. According to the XRD patterns (Fig. 7) ilmenite milled in air for 10 hours showed $FeTiO_3$ as the dominant phase while the sample milled for 100 hours showed the presence of a new phase β-$Fe_2Ti_3O_9$ which has the chemical composition of pseudorutile ($Fe_2Ti_3O_9$), but a different crystalline structure.

Ilmenite oxidizes in air as follows,

$$6\ FeTiO_3(S) + 3/2\ O_2(g) = 2\ \beta\text{-}Fe_2Ti_3O_9(S) + Fe_2O_3(S)$$

The spectrum of the natural sample showed two doublets where the first doublet corresponds to Fe^{2+} attributed to the $FeTiO_3$ phase, and the second doublet is a Fe^{3+} resonance that is associated with the α- $Fe_2Ti_3O_9$ pseudorutile (Fig. 8). The Fe^{2+}: Fe^{3+} was found to be 1:1 which is also consistent with the XRF data. The predominant doublet for the ilmenite milled for 200 hours is consistent with the Mossbauer spectrum for Fe^{2+}. The presence of Fe^{2+} is due to the reductive transformation of α-$Fe_2Ti_3O_9$ to $FeTiO_3$ due to the presence of Fe as a contaminant in the milling process. However, in contrast, ilmenite milled for 100 hours in air showed the presence of Fe^{3+} due to the partial oxidation of ilmenite. Further, the concentration Fe^{3+} was found to decrease and that of Fe^{2+}

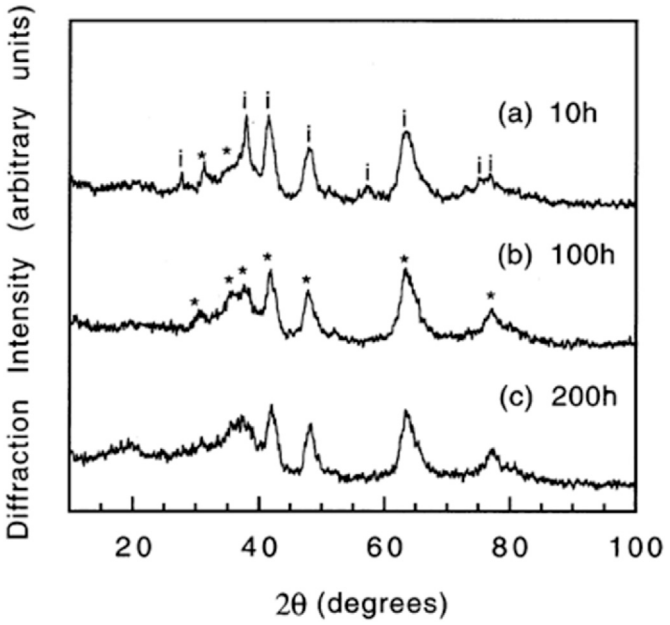

Fig. 7. XRD patterns for the ilmenite samples milled at (a) 10 hours (b) 100 hours (c) 200 hours. (i-$FeTiO_3$; * β-$Fe_2Ti_3O_9$). Adapted from Ref. [72].

increased with increasing milling time of ilmenite milled in a vacuum. Ilmenite milled in air showed a different behaviour where the Fe^{2+}appeared to be converted to Fe^{3+}. Mossbauer spectra showed that during ball milling in vacuum, ilmenite gets reduced while on milling in air it is oxidized. In another study, the product obtained on milling ilmenite in vacuum for extended hours (200 hours) completely dissolved in sulfuric acid because Fe^{3+} (of α- $Fe_2Ti_3O_9$) was reduced to Fe^{2+} ($FeTiO_3$). It has been found that the $FeTiO_3$ phase can be more easily dissolved than $Fe_2Ti_3O_9$ in sulfuric acid [72]. Ilmenite milled in air showed only 69% dissolution even with extended milling hours due to the oxidation of $FeTiO_3$ to β-$Fe_2Ti_3O_9$. The surface area reached a maximum of 9.2 m^2/g on milling the sample for 15 hours. The surface area decreased to almost the same as the initial surface area (before milling) after milling for 200 hours in vacuum. The rapid increase in surface area during the first stage was due to the breakdown of the ilmenite particles and with prolonged milling surface area has decreased due to agglomeration of the small particles [72]. Welham et al. [73] also reported the same trend in surface area when ilmenite was milled. They observed that the surface area increased with increasing milling time up to 10 hours and then decreased to a value below that of the starting

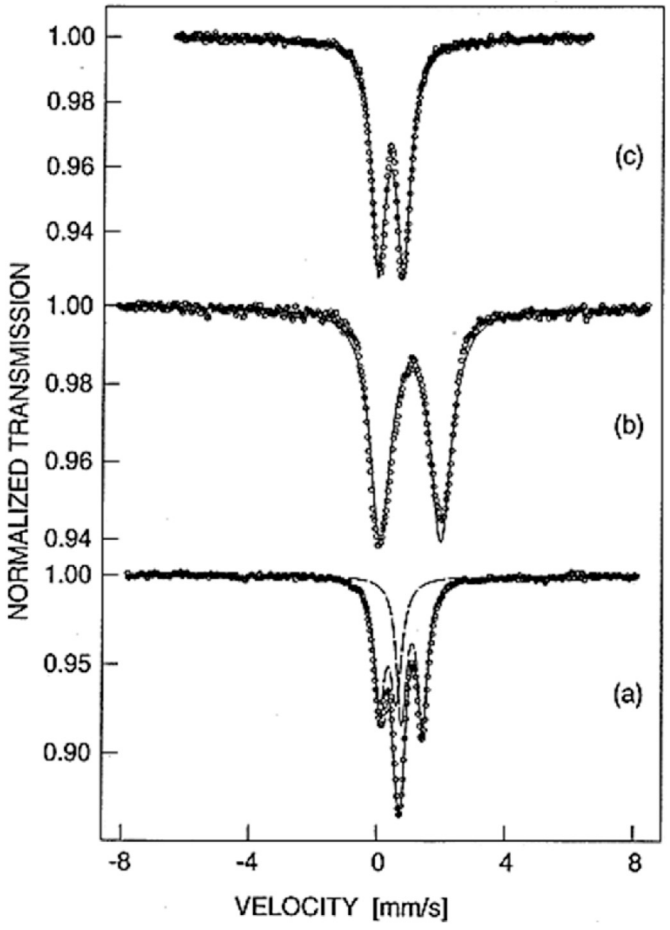

Fig. 8. Room Temperature Mossbauer spectra for ilmenite samples (a) starting ilmenite material (b) milled in vacuum for 200 hours (c) milled in air for 100 hours. Adapted from Ref. [72].

material. The increase is attributed to the increase in surface area due to particle breakage during the early stage and the decrease in realloying of small particles and particle agglomeration [73].

The effect of mechanical activation on leaching kinetics of Panzhihua ilmenite had been studied [74]. It has been found that ball milling partially activates ilmenite because milled ilmenite showed a rapid dissolution in 50% sulfuric acid initially. Thereafter, the rate of leaching decreased suggesting that only a part of the ilmenite had been milled to produce fine particles with high surface area, the rest remaining the same as the unmilled ilmenite. Thus, it is evident that energetic milling enhances the dissolution of ilmenite by increasing the surface area and elevating its chemical activity [75]. The activation energy for the initial dissolution stage was low because the dissolution of both fine particles and highly reactive crystal faces occur. The activation energy reaches that of the unmilled ilmenite at the later stage due to the consumption of fine particles and crystal faces. Partial activation of ilmenite by ball milling was also reported [76]. The authors state that simultaneous milling and leaching significantly increased the dissolution of Panzihihua ilmenite to 80% when ilmenite is mixed with 50% sulfuric acid in an industrial ore/acid ratio and heated to 120 °C for 2 hours. Though an 80% dissolution was achieved it was lower than for the commercial conversion due to the hydrolysis of titanium. This could be minimized by using lower temperatures for prolonged hours [65]. Interestingly, there are two types of structural defects induced by ball milling, namely effective defects and ineffective defects. The strain in the c-axis of the ilmenite unit cell strongly affects the leaching rate in effective defects while the strain in the a-axis has minimal effect on the leaching rate in ineffective defects [74]. Dissolution kinetics of Panzhihua ilmenite were also reported [76–78]. According to Welham et al. [73], leaching of milled ilmenite takes place in two stages where a rapid dissolution is followed by a slower reaction. The production of small crystals at the early stage renders a rapid dissolution of ilmenite at the first stage. Further, preferential exposure of the main parting planes [79], where separation occurs along with a lamellar twin due to application of pressure during milling is also responsible for the increased dissolution. The initial mass transport controlled dissolution may have occurred as the large fraction of these planes exposed on small crystallites results in high surface energy per volume and therefore high reactivity. In the second less reactive stage, the chemically controlled reaction occurred when the less reactive planes were exposed to unmilled ilmenite. The main effect of prolonged milling on the dissolution of ilmenite is to enhance the mass transport controlled step because milling increases the number of grain boundaries [73].

The effect of ball milling on acid leaching of titanium and iron from ilmenite was also studied by using ilmenite found in Chatrapur, India [80]. Unmilled ilmenite consists predominantly of ilmenite with minor amounts of pseudo-rutile. Pseudo-rutile phase disappears due to amorphization upon milling for 240 minutes. The particle size of the unmilled sample varied between 100 and 500 μm. As shown in Fig. 9, the particle size of the milled sample decreased with the time of milling and reached a range of 40 to 0.4 μm after milling for 90 minutes. The surface area increased exponentially and reached a maximum of 4 m^2/g after milling for 240 minutes. Further, the crystallite size decreased with increasing milling time, while the strain increased linearly with time. Complete oxidation of Fe^{2+} to Fe^{3+} in the mechanically activated sample was achieved in ambient air upon heating at 850 °C while only 50% oxidation occurred in the unmilled sample. The ilmenite phase was absent in the annealed activated sample. It contains only pseudo-rutile, rutile and pseudo-brookite phases. In the annealed unmilled sample unoxidized ilmenite was present in addition to pseudo-rutile and pseudo-brookite. Particle size exponentially decreased and remained constant after 90 minutes of milling, and the surface area was found to increase continuously with increasing milling time. Leaching of milled ilmenite in 9.4 M sulfuric acid at temperatures of 80, 95, 120 °C for varying durations (30–240 minutes) indicated that leaching increases with time and temperature of leaching. A maximum of 65% titanium and 90% Fe leached in the sample milled for 240 minutes when treated at 120 °C for 4 hours as shown in Fig. 10. The leaching of iron was greater than that of titanium at all temperatures. Fe^{2+} and Ti^{4+} both complex with six water molecules during solvation. $Ti(H_2O)_6^{4+}$ is unstable. Further complexation occurs and Ti^{4+} forms the stable $Ti^{4+}(OH^-)_2(SO_4^{2-})(H_2O)_3$ complex *via* ligand exchange reaction. This complex is equivalent to the oxysulfate complex given in the following reaction which indicates the

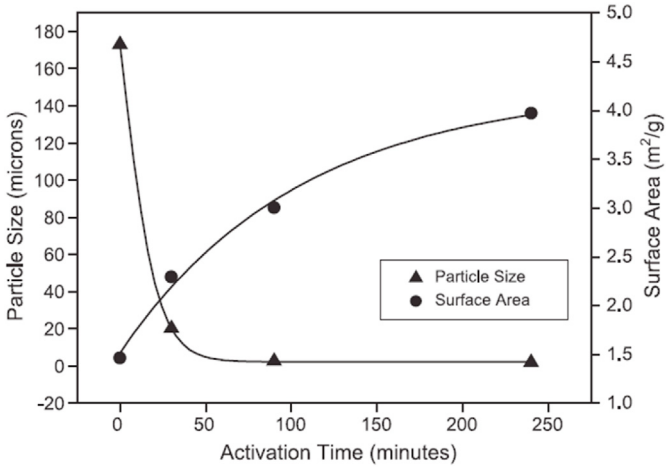

Fig. 9. Variation of the particle size and the surface area with increasing milling time. Adapted from Ref. [80].

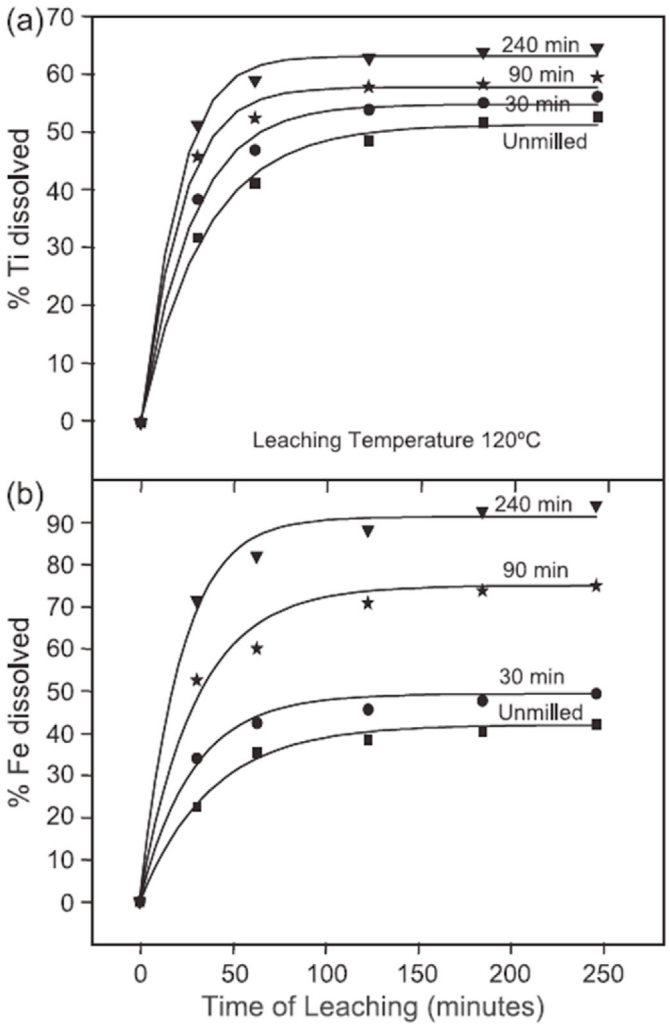

Fig. 10. Variation of (a) Ti (b) Fe with leaching time at 120 °C. Adapted from Ref. [80].

dissolution of ilmenite. The formation of this complex retards the dissolution of Ti^{4+}. However, the dissolution of Fe^{2+} is not affected [80].

$$FeTiO_3(S) + SO_4^{2-}(S) + 4H^+(aq) = Fe^{2+}(aq) + TiO{\cdot}SO_4(aq) + 2H_2O(L)$$

In addition to the increase in the impact of surface area on the increased dissolution of milled ilmenite several other factors such as structural disorders [81], amorphization of material [82], formation of new phases which are amendable to leaching [83], enhanced strains [84], and preferential dissolution of select crystal faces [79] can contribute to the ore dissolution.

3.3. Treatment in hydrochloric acid and sulfuric acid

Interestingly Sasikumar et al. [85] have performed a similar study on the effect of mechanical activation on the dissolution of ilmenite in HCl and H_2SO_4 where the origin of ilmenite is different. The authors have collected ilmenite from the Manavalakurichi site in India. The composition of this ilmenite was different with much higher Fe^{3+}/Fe^{2+} content. This is directly reflected by the presence of a higher amount of pseudo-rutile ($Fe_2Ti_3O_9$) phase. Further, the pseudo-rutile phase is present in the amorphous form unlike in the Chatrapur ilmenite in which the amorphization of the pseudo-rutile phase occurred during ball milling. This was attributed to the weathering processes. Dissolution of both iron and titanium of unmilled ilmenite in HCl was found to increase with increasing time and increasing temperature of dissolution. However, though the dissolution of iron increased with time and temperature of dissolution, the dissolution of titanium was found to be affected by the hydrolysis of $TiOCl_2$, precipitation of $Ti(OH)_4$ at higher temperatures and low acid concentrations for prolonged periods of leaching. This was different from leaching in sulfuric acid where the dissolution of both iron and titanium of both milled and unmilled ilmenite increased with increasing time, temperature and acid concentration of leaching. The leaching of iron and titanium in both HCl and H_2SO_4 was higher for milled samples than unmilled samples. The dissolution kinetics in both HCl and H_2SO_4 were found to agree with the reaction rate control mechanism initially and thereafter follows the shrinking core model where product layer diffusion is rate controlling. The activation energy of dissolution of both iron and titanium in H_2SO_4 was found to be higher for the first stage of dissolution and lower for the second stage. The trend was the same for the dissolution of both iron and titanium in HCl. The activation energy for the dissolution of titanium for the second stage was not defined due to the hydrolysis and precipitation. The activation energies for the dissolution of iron and titanium monotonically increased with increasing time of milling. It was concluded that the mechanical activation has caused an increase in the dissolution of ilmenite in acid due to the enhancement of surface area and structural disorders [85].

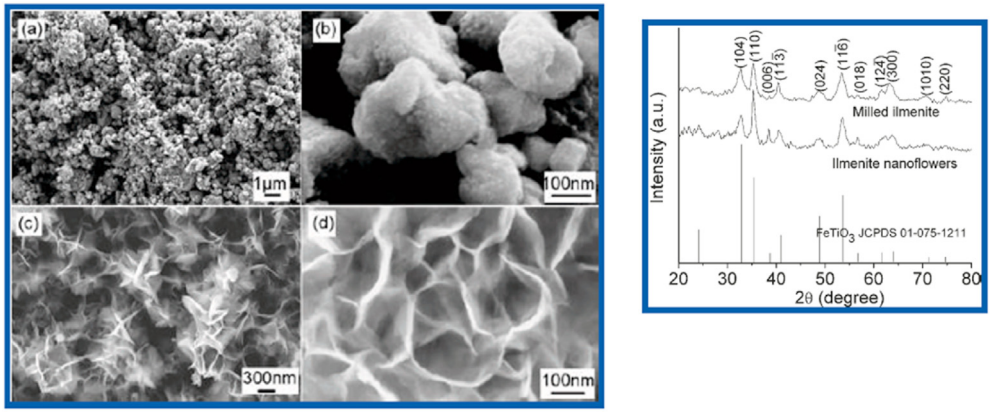

(i) (ii)

Fig. 11. (i) SEM images of ball-milled sample (a,b) and the same sample after the hydrothermal treatment in NaOH (c,d). SEM images have been collected by using Carl Zeiss supra55vp instrument (ii) XRD patterns of the milled $FeTiO_3$ and the resulting flowerlike nanostructures. Strong lines from the JCPDS 01-075-1211 are also shown at the bottom of the graph. Adapted from Ref. [86].

4. Ball milling and hydrothermal treatment

Ball milling followed by hydrothermal treatment with NaOH is a remarkable technique to produce different nanostructures from mineral ilmenite. Tao et al. [86] reported the production of $FeTiO_3$ nanoflowers from natural ilmenite by mechanical activation followed by hydrothermal treatment in NaOH. Briefly, ilmenite powder from Australia was ball milled under an Ar atmosphere at a pressure of 100 kPa for 150 hours at room temperature, hydrothermally treated at 120 °C for 2 hours in 2 M NaOH followed by drying at 90 °C. According to the SEM images shown in Fig. 6, the milled sample consists predominantly of submicrometer agglomerates (Fig. 11 (i) a) and such agglomerates consist of aggregates of small particles as shown in Fig. 11 (i) b. After treatment with NaOH uniform flowerlike architectures of about 1–2 μm are produced where petals of 5–20 nm thickness and 100–200 nm width are interconnected (Fig. 11 (i) c and d). The X-ray diffraction pattern of the nanoflowers (Fig. 11 (ii)) is quite similar to that of milled ilmenite and agreed well with the standard XRD pattern for $FeTiO_3$ (JCPDS 01-075-1211). It is suggested that nanoflowers are formed *via* a dissolution-precipitation process where the primary particles which are the aggregates are formed during ball milling and the secondary stage of growth has taken place *via* Oswald ripening where the small particles dissolve into solution and the dissolved material reprecipitates on growing crystallites leading to the formation of large structures. Further, it was found that NaOH is essential to the formation of such flowerlike structures because the milled ilmenite that was hydrothermally treated under the same conditions using water instead of NaOH did not produce flowerlike structures. The authors of this study are in the view that the sodium titanate which forms by the chemical reactions between $FeTiO_3$ and NaOH is water-soluble for the dissolution-precipitation mechanism to take place. Moreover, the $FeTiO_3$ flower-like structures produced were found to be an effective electrode material when tested as a supercapacitor [86].

Hydrometallurgical processing of ilmenite was attained through leaching in NaOH solution after mechanical activation under high temperature and high pressure [87]. Ilmenite found from Rosetta, Egypt was milled in NaOH solution using steel balls with a diameter of 2.0 mm at a rotation speed of 1200 min^{-1}. The degree of leaching was evaluated by dissolving the iron titanium mixture in HCl. Reactions of ilmenite with sodium hydroxide and the iron titanium cake with HCl are given below,

$$4FeTiO_3(S) + 8\ NaOH(aq) + O_2^-\ (aq) = 4\ Na_2TiO_3(S) + 2\ Fe_2O_3(S) + 4H_2O(L)$$

$$Na_2TiO_3(S) + FeO(S) + 6HCl(aq) = TiOCl_2(aq) + FeCl_2(aq) + 2\ NaCl(aq) + 3H_2O(L)$$

Briefly, aqueous oxygen is transported to the surface of ilmenite grains via convection and diffusion where the oxygen molecules dissociate to oxygen ions at the surface of ilmenite,

$$O_{2(aq)} + 4e = 2O^{2-}(aq)$$

The oxygen ions and electrons are then transported to the reacting boundaries through the surface of the ilmenite. Thereafter, TiO_2 reacts with sodium hydroxide to produce sodium titanate,

$$2TiO_2(S) + 4NaOH(aq) = 2Na_2TiO_3(S) + 4H_2O(L)$$

X-ray diffraction patterns of the products obtained at 150, 170 and 200 °C showed that the reaction of ilmenite with sodium hydroxide has taken place via the formation of $Na_2Fe_2Ti_3O_{10}$ and $Na_2Ti_2Ti_6O_{16}$ phases. When the produced sodium titanate was washed with 30% HCl, the dried product showed the presence of anatase which converted to a mixture of anatase and rutile when calcined at 800 °C and only rutile when calcined at 900 °C, with a chemical composition of 98.8% TiO_2 and 0.7% of Fe_2O_3. It was found that extraction of Ti increased with increasing temperature of leaching in the range of 140–220 °C and this trend was also observed for other parameters such as varying NaOH concentration (0.1 M − 0.5 M in 0.1 M increments) and varying oxygen partial pressure (from 1 to 6 bars in 1 bar increments). Further, increasing the time of grinding from 0 to 4 hours in 1 hour increments, increased the dissolution of ilmenite. The finer the particles of ilmenite, the higher the efficiency of extraction of Ti [87].

Rajakaruna et al. [88] reported the synthesis of TiO_2 from natural ilmenite by a combination of several methods including magnetic separation, ball milling, revolving acid hydrothermal process, a stationary base hydrothermal process followed by calcination. The ilmenite sample was run through a magnetic separator to separate ilmenite from other mineral sand and was subjected to ball milling to reduce the particle size to around 100 μm. Iron has been leached during the revolving acid hydrothermal treatment performed at 170 °C for 3 hours using 6 M HCl. The inside pressure in a closed system of an autoclave is much higher and facilitates the breakage of the lattice. This eliminates the problem associated with the chloride process where both iron and titanium dissolve in high concentrations of acid and low temperatures. A low concentration of acid and high temperature is required to minimize titanium dissolution [89,90]. However, in an open system, the breakage of the lattice is unfavourable and hence, a high acid concentration and a high temperature are required. However, from the revolving acid hydrothermal method titanium dioxide can be precipitated in its polymer forms as given in the following reactions.

$$TiOCl_4^{2-}\ (aq) + (1+n)\ H_2O\ (l) = TiO_2.nH_2O\ (s) + 2H^+\ (aq) + 2Cl^-\ (aq)$$

$$TiOCl_2\ (aq) + H_2O\ (l) = 2\ HCl\ (aq) + H_2TiO_3\ (s)$$

Magnetic separation does not remove the silica impurities and refluxing in 0.5 M NaOH together with hydrogen peroxide was performed to remove the silica. Ti species (TiO_2 and H_2TiO_3) react as shown in the following reactions but silica remained undissolved.

$$TiO_2.nH_2O\ (s) + H_2O_2\ (l) + NaOH\ (aq) = Na_xTi(O_2)_i(OH)_j\ (aq) + nH_2O\ (l)$$

$$H_2TiO_3\ (s) + H_2O_2\ (l) + NaOH\ (aq) = Na_xTi(O_2)_i(OH)_j\ (aq) + H_2O\ (l)$$

The resulting titanium sol has been subjected to hydrothermal treatment with hexadecyltrimethylammonium bromide at a high concentration than its critical micelle concentration. This has produced flower-like $Na_2Ti_3O_7$ structures. Once the medium is made acidic $H_2Ti_3O_7$ (s) is produced as follows,

$$Na_2Ti_3O_7\ (s) + 2H^+\ (aq) = H_2Ti_3O_7\ (s) + 2Na^+\ (aq)$$

When the product is heated to 150 °C amorphous TiO_2 is formed as given in the reaction below, and calcining the product at 350 °C and 650 °C resulting anatase phase and rutile phases, respectively [88].

$$H_2Ti_3O_7\ (s) = 3\ TiO_2 + H_2O\ (l)$$

5. Conclusions

The ball milling process creates textural and crystallographic changes in ilmenite. Generally, mechanical activation reduces the particle size and crystallite size, and increase the surface area. With different reducing agents like activated carbon, sulfur and graphite, ilmenite produce compounds such as TiO_2, Ti_3O_9, FeS_2, Fe_9S_{10}, and Fe, while $Fe_2Ti_3O_9$ and Fe_2TiO_5 are produced without any reducing agent when ilmenite is annealed to high temperatures in the range of 400–1400 °C. Mechanical activation enhances the digestion of ilmenite in acids including hydrochloric acid and sulfuric acid, and improve the reactivity of ilmenite when hydrothermally treated.

Funding

This research was supported by the Accelerating Higher Education Expansion and Development (AHEAD) Operation of the Ministry of Higher Education funded by the World Bank.

Declaration of competing interest

The authors report no conflict of interest.

References

[1] F. Moosakazemi, M.R. Tavakoli Mohammadi, M. Mohseni, M. Karamoozian, M. Zakeri, Effect of design and operational parameters on particle morphology in ball mills, Int. J. Miner. Process. 165 (Aug. 2017) 41–49, https://doi.org/10.1016/j.minpro.2017.06.001.

[2] R. Černý, et al., Trimetallic borohydride Li3MZn5(BH4) 15 (M = Mg, Mn) containing two weakly interconnected frameworks, Inorg. Chem. 52 (17) (Sep. 2013) 9941–9947, https://doi.org/10.1021/ic401139k.

[3] D.B. Ravnsbæk, et al., Novel alkali earth borohydride Sr(BH4)2 and borohydride-chloride Sr(BH4)Cl, Inorg. Chem. 52 (19) (Oct. 2013) 10877–10885, https://doi.org/10.1021/ic400862s.

[4] J. Huot, D.B. Ravnsbæk, J. Zhang, F. Cuevas, M. Latroche, T.R. Jensen, Mechanochemical synthesis of hydrogen storage materials, Prog. Mater. Sci. 58 (1) (Jan. 01, 2013) 30–75, https://doi.org/10.1016/j.pmatsci.2012.07.001. Elsevier Ltd.

[5] M.B. Ley, et al., LiCe(BH 4) 3Cl, a new lithium-ion conductor and hydrogen storage material with isolated tetranuclear anionic clusters, Chem. Mater. 24 (9) (May 2012) 1654–1663, https://doi.org/10.1021/cm300792t.

[6] D.B. Ravnsbæk, L.H. Sørensen, Y. Filinchuk, F. Besenbacher, T.R. Jensen, Screening of metal borohydrides by mechanochemistry and diffraction, Angew. Chem. Int. Ed. 51 (15) (Apr. 2012) 3582–3586, https://doi.org/10.1002/anie.201106661.

[7] C.C. Piras, S. Fernández-Prieto, W.M. De Borggraeve, Ball milling: a green technology for the preparation and functionalisation of nanocellulose derivatives, Nanoscale Adv. 1 (3) (Mar. 12, 2019) 937–947, https://doi.org/10.1039/c8na00238j. Royal Society of Chemistry.

[8] • Titanium production worldwide by country 2020 | Statista. https://www.statista.com/statistics/759972/mine-production-titanium-minerals-worldwide-by-country/. (Accessed 28 August 2021).

[9] M.H.H. Mahmoud, A.A.I. Afifi, I.A. Ibrahim, Reductive leaching of ilmenite ore in hydrochloric acid for preparation of synthetic rutile, Hydrometallurgy 73 (1–2) (Apr. 2004) 99–109, https://doi.org/10.1016/j.hydromet.2003.08.001.

[10] M.G. Shahien, M.M.H. Khedr, A.E. Maurice, A.A. Farghali, R.A.M. Ali, Synthesis of high purity rutile nanoparticles from medium-grade Egyptian natural ilmenite, Beni-Suef Univ. J. Basic Appl. Sci. 4 (3) (Sep. 2015) 207–213, https://doi.org/10.1016/j.bjbas.2015.05.013.

[11] A.M. Ramadan, M. Farghaly, W.M. Fathy, M.M.M. Ahmed, Leaching and Kinetics Studies on Processing of Abu-Ghalaga Ilmenite Ore, 2016.

[12] L. Palliyaguru, N.D.H. Arachchi, C.D. Jayaweera, P.M. Jayaweera, Production of synthetic rutile from ilmenite via anion-exchange, Miner. Process. Extr. Metall. Trans. Inst. Min. Metall. 127 (3) (Jul. 2018) 169–175, https://doi.org/10.1080/03719553.2017.1331621.

[13] T.S. Mackey, Upgrading ilmenite into a high-grade synthetic rutile, JOM (J. Occup. Med.) 46 (4) (Apr. 1994) 59–64, https://doi.org/10.1007/BF03220676.

[14] S. Mohammad Ali, Production of Nanosized Synthetic Rutile from Ilmenite Concentrate by Sonochemical HCl and H 2 SO 4 Leaching, " Iranian Institute of Research and Development in Chemical Industries (IRDCI)-ACECR, Jun, 2014, https://doi.org/10.30492/IJCCE.2014.10749.

[15] A. Miyoshi, S. Nishioka, K. Maeda, Water splitting on rutile TiO $_2$ -based photocatalysts, Chem. Eur J. 24 (69) (Dec. 2018) 18204–18219, https://doi.org/10.1002/chem.201800799.

[16] A. Wolcott, W.A. Smith, T.R. Kuykendall, Y. Zhao, J.Z. Zhang, Photoelectrochemical water splitting using dense and aligned TiO $_2$ nanorod arrays, Small 5 (1) (Jan. 2009) 104–111, https://doi.org/10.1002/smll.200800902.

[17] A.J. Cowan, J. Tang, W. Leng, J.R. Durrant, D.R. Klug, Water splitting by nanocrystalline TiO 2 in a complete photoelectrochemical cell exhibits efficiencies limited by charge recombination, J. Phys. Chem. C 114 (9) (Mar. 2010) 4208–4214, https://doi.org/10.1021/jp909993w.

[18] M.M. Haque, M. Muneer, TiO2-mediated photocatalytic degradation of a textile dye derivative, bromothymol blue, in aqueous suspensions, Dyes Pigments 75 (2) (Jan. 2007) 443–448, https://doi.org/10.1016/j.dyepig.2006.06.043.

[19] B. Neppolian, H.C. Choi, S. Sakthivel, B. Arabindoo, V. Murugesan, Solar light induced and TiO2 assisted degradation of textile dye reactive blue 4, Chemosphere 46 (8) (2002) 1173–1181, https://doi.org/10.1016/S0045-6535(01)00284-3. Mar.

[20] I. Poulios, I. Aetopoulou, Photocatalytic degradation of the textile dye reactive orange 16 in the presence of tio2 suspensions, Environ. Technol. (United Kingdom) 20 (5) (May 1999) 479–487, https://doi.org/10.1080/09593332008616843.

[21] S. Sarkar, S. Chakraborty, C. Bhattacharjee, Photocatalytic degradation of pharmaceutical wastes by alginate supported TiO2 nanoparticles in packed bed photo reactor (PBPR), Ecotoxicol. Environ. Saf. 121 (Nov. 2015) 263–270, https://doi.org/10.1016/j.ecoenv.2015.02.035.

[22] Y. He, N.B. Sutton, H.H.H. Rijnaarts, A.A.M. Langenhoff, Degradation of pharmaceuticals in wastewater using immobilized TiO2 photocatalysis under simulated solar irradiation, Appl. Catal. B Environ. 182 (Mar. 2016) 132–141, https://doi.org/10.1016/j.apcatb.2015.09.015.

[23] H. Yang, G. Li, T. An, Y. Gao, J. Fu, Photocatalytic degradation kinetics and mechanism of environmental pharmaceuticals in aqueous suspension of TiO2: a case of sulfa drugs, Catal. Today 153 (3–4) (Aug. 2010) 200–207, https://doi.org/10.1016/j.cattod.2010.02.068.

[24] Z. Mengyue, C. Shifu, T. Yaowu, Photocatalytic degradation of organophosphorus pesticides using thin films of TiO2, J. Chem. Technol. Biotechnol. 64 (4) (Dec. 1995) 339–344, https://doi.org/10.1002/jctb.280640405.

[25] X. Zhu, C. Yuan, Y. Bao, J. Yang, Y. Wu, Photocatalytic degradation of pesticide pyridaben on TiO2 particles, J. Mol. Catal. A Chem. 229 (1–2) (Mar. 2005) 95–105, https://doi.org/10.1016/j.molcata.2004.11.010.

[26] K.H. Ko, Y.C. Lee, Y.J. Jung, Enhanced efficiency of dye-sensitized TiO2 solar cells (DSSC) by doping of metal ions, J. Colloid Interface Sci. 283 (2) (Mar. 2005) 482–487, https://doi.org/10.1016/j.jcis.2004.09.009.

[27] M. Bhogaita, S. Yadav, A.U. Bhanushali, A.A. Parsola, R. Pratibha Nalini, Synthesis and characterization of TiO2 thin films for DSSC prototype, Mater. *Today: Proceedings* 3 (6) (Jan. 2016) 2052–2061, https://doi.org/10.1016/j.matpr.2016.04.108.

[28] T. Song, U. Paik, TiO2 as an active or supplemental material for lithium batteries, J. Mater. Chem. 4 (1) (Dec. 15, 2015) 14–31, https://doi.org/10.1039/c5ta06888f. Royal Society of Chemistry.

[29] S.S. El-Deen, et al., Anatase TiO2 nanoparticles for lithium-ion batteries, Ionics (Kiel). 24 (10) (Oct. 2018) 2925–2934, https://doi.org/10.1007/s11581-017-2425-y.

[30] J.H. Braun, A. Baidins, R.E. Marganski, TiO2 pigment technology: a review, Prog. Org. Coating 20 (2) (May 1992) 105–138, https://doi.org/10.1016/0033-0655(92)80001-D.

[31] F. Shao, J. Sun, L. Gao, J. Chen, S. Yang, Electrophoretic deposition of TiO2 nanorods for low-temperature dye-sensitized solar cells, RSC Adv. 4 (15) (Jan. 2014) 7805–7810, https://doi.org/10.1039/C3RA47286H.

[32] I. Dundar, M. Krichevskaya, A. Katerski, I.O. Acik, TiO2 thin films by ultrasonic spray pyrolysis as photocatalytic material for air purification, R. Soc. Open Sci. 6 (2) (Feb. 2019), https://doi.org/10.1098/RSOS.181578.

[33] H. Arami, M. Mazloumi, R. Khalifehzadeh, and S. K. Sadrnezhaad, "Sonochemical preparation of TiO2 nanoparticles," Mater. Lett., vol. 61, no. 23–24, pp. 4559–4561, Sep. 2007, doi: 10.1016/J.MATLET.2007.02.051.

[34] G.S. Falk, M. Borlaf, M.J. López-Muñoz, J.C. Fariñas, J.B. Rodrigues Neto, R. Moreno, Microwave-assisted synthesis of TiO2 nanoparticles: photocatalytic activity of powders and thin films, J. Nanoparticle Res. 20 (2) (Jan. 2018) 1–10, https://doi.org/10.1007/S11051-018-4140-7.

[35] O.L. Kang, A. Ahmad, U.A. Rana, N.H. Hassan, Sol-gel titanium dioxide nanoparticles: preparation and structural characterization, J. Nanotechnol. 2016 (2016), https://doi.org/10.1155/2016/5375939.

[36] A.C. Nkele, et al., A study on titanium dioxide nanoparticles synthesized from titanium isopropoxide under SILAR-induced gel method: transition from anatase to rutile structure, Inorg. Chem. Commun. 112 (Feb. 2020) 107705, https://doi.org/10.1016/J.INOCHE.2019.107705.

[37] M. Darvishi, J. Seyed-Yazdi, Characterization and comparison of photocatalytic activities of prepared TiO2/graphene nanocomposites using titanium butoxide and TiO2 via microwave irradiation method, Mater. Res. Express 3 (8) (Aug. 2016), https://doi.org/10.1088/2053-1591/3/8/085601, 085601.

[38] W. Shi, A.H. Park, S. Xu, P.J. Yoo, Y.U. Kwon, Continuous and conformal thin TiO2-coating on carbon support makes Pd nanoparticles highly efficient and durable electrocatalyst, Appl. Catal. B Environ. 284 (May 2021) 119715, https://doi.org/10.1016/J.APCATB.2020.119715.

[39] N. Watanabe, T. Kaneko, Y. Uchimaru, S. Yanagida, A. Yasumori, Y. Sugahara, Preparation of water-dispersible TiO2 nanoparticles from titanium tetrachloride using urea hydrogen peroxide as an oxygen donor, CrystEngComm 15 (48) (Nov. 2013) 10533–10540, https://doi.org/10.1039/C3CE41561A.

[40] R.G. Haverkamp, D. Kruger, R. Rajashekar, The digestion of New Zealand ilmenite by hydrochloric acid, Hydrometallurgy 163 (Aug. 2016) 198–203, https://doi.org/10.1016/j.hydromet.2016.04.015.

[41] K.N. Han, T. Rubcumintara, M.C. Fuerstenau, Leaching behavior of ilmenite with sulfuric acid, Metall. Trans. B 18 (2) (Jun. 1987) 325–330, https://doi.org/10.1007/BF02656150.

[42] X. Xiong, Z. Wang, F. Wu, X. Li, H. Guo, Preparation of TiO2 from ilmenite using sulfuric acid decomposition of the titania residue combined with separation of Fe3 + with EDTA during hydrolysis, Adv. Powder Technol. 24 (1) (2013) 60–67, https://doi.org/10.1016/j.apt.2012.02.002.

[43] Z. Li, Z. Wang, G. Li, Preparation of nano-titanium dioxide from ilmenite using sulfuric acid-decomposition by liquid phase method, Powder Technol. 287 (2016) 256–263, https://doi.org/10.1016/j.powtec.2015.09.008.

[44] A. Simpraditpan, T. Wirunmongkol, S. Pavasupree, W. Pecharapa, Hydrothermal synthesis of nanofibers from natural ilmenite mineral and their utilization for dye-sensitized solar cell, Integrated Ferroelectrics Int. J. 149 (1) (2013) 135–142, https://doi.org/10.1080/10584587.2013.853592.

[45] A. Simpraditpan, T. Wirunmongkol, S. Pavasupree, W. Pecharapa, Simple hydrothermal preparation of nanofibers from a natural ilmenite mineral, Ceram. Int. 39 (3) (Apr. 2013) 2497–2502, https://doi.org/10.1016/j.ceramint.2012.09.008.

[46] Y. Liu, T. Qi, J. Chu, Q. Tong, Y. Zhang, Decomposition of ilmenite by concentrated KOH solution under atmospheric pressure, Int. J. Miner. Process. 81 (2) (2006) 79–84, https://doi.org/10.1016/j.minpro.2006.07.003.

[47] V. Kordzadeh-Kermani, M. Schaffie, H. Hashemipour Rafsanjani, M. Ranjbar, A modified process for leaching of ilmenite and production of TiO2 nanoparticles,

Hydrometallurgy 198 (2020) 105507, https://doi.org/10.1016/j.hydromet.2020.105507.
[48] T.H. Nguyen, M.S. Lee, A review on the recovery of titanium dioxide from ilmenite ores by direct leaching technologies, Miner. Process. Extr. Metall. Rev. 40 (4) (Jul. 04, 2019) 231–247, https://doi.org/10.1080/08827508.2018.1502668. Taylor and Francis Inc.
[49] W. Zhang, Z. Zhu, C.Y. Cheng, A literature review of titanium metallurgical processes, Hydrometallurgy 108 (3–4) (Jul. 2011) 177–188, https://doi.org/10.1016/J.HYDROMET.2011.04.005.
[50] W.J. Bruckard, M.I. Pownceby, L.K. Smith, G.J. Sparrow, Review of processing conditions for Murray Basin ilmenite concentrates 124 (1) (Mar. 2014) 47–63, https://doi.org/10.1179/1743285514Y.0000000083.
[51] V.A. Sadykov, et al., "Advanced Materials for Solid Oxide Fuel Cells and Membrane Catalytic Reactors," in *Advanced Nanomaterials for Catalysis and Energy: Synthesis, Characterization and Applications*, Elsevier, 2018, pp. 435–514.
[52] M. Awano, H. Takagi, Y. Kuwahara, Grinding effects on the synthesis and sintering of cordierite, J. Am. Ceram. Soc. 75 (9) (Sep. 1992) 2535–2540, https://doi.org/10.1111/j.1151-2916.1992.tb05608.x.
[53] C. Sasikumar, S. Srikanth, N.K. Mukhopadhyay, S.P. Mehrotra, Energetics of mechanical activation - application to ilmenite, Miner. Eng. 22 (6) (May 2009) 572–574, https://doi.org/10.1016/j.mineng.2009.01.013.
[54] P. Baláž, Extractive Metallurgy of Activated Minerals, Elsevier, 2000.
[55] Y. Chen, T. Hwang, M. Marsh, J.S. Williams, Mechanically activated carbothermic reduction of ilmenite, Metall. Mater. Trans. A Phys. Metall. Mater. Sci. 28 (5) (1997) 1115–1121, https://doi.org/10.1007/s11661-997-0277-1.
[56] Y. Chen, T. Hwang, J.S. Williams, Ball milling induced low-temperature carbothermic reduction of ilmenite, Mater. Lett. 28 (1–3) (Sep. 1996) 55–58, https://doi.org/10.1016/0167-577X(96)00026-2.
[57] Y. Chen, Low-temperature oxidation of ilmenite (FeTiO3) induced by high energy ball milling at room temperature, J. Alloys Compd. 257 (1–2) (Jul. 1997) 156–160, https://doi.org/10.1016/S0925-8388(97)00012-1.
[58] I.E. Gney, A.F.R. Csiro, The Structure of Pseudorutile and its Role in the Natural Alteration of Llmenite, 1975.
[59] R.A. Briggs, A. Sacco, The oxidation of llmenite and its relationship to the FeO-Fe2O3-TiO2 phase diagram at 1073 and 1140 K, Metall. Trans. A 24 (6) (Jun. 1993) 1257–1264, https://doi.org/10.1007/BF02668194.
[60] Y. Chen, Different oxidation reactions of ilmenite induced by high energy ball milling, J. Alloys Compd. 266 (1–2) (Feb. 1998) 150–154, https://doi.org/10.1016/S0925-8388(97)00494-5.
[61] Y. Chen, M. Marsh, J.S. Williams, B. Ninham, Production of rutile from ilmenite by room temperature ball-milling-induced sulphurisation reaction, J. Alloys Compd. 245 (1–2) (Nov. 1996) 54–58, https://doi.org/10.1016/S0925-8388(96)02483-8.
[62] M. Chen, A.T. Tang, X. Xiao, Effect of milling time on carbothermic reduction of ilmenite, Trans. Nonferrous Met. Soc. China (English Ed. 25 (12) (Dec. 2015) 4201–4206, https://doi.org/10.1016/S1003-6326(15)64070-5.
[63] T. Tao, et al., Expanding the applications of the ilmenite mineral to the preparation of nanostructures: TiO $_2$ nanorods and their photocatalytic properties in the degradation of oxalic acid, Chem. Eur J. 19 (3) (Jan. 2013) 1091–1096, https://doi.org/10.1002/chem.201202451.
[64] T. Tao, et al., Porous TiO2 with a controllable bimodal pore size distribution from natural ilmenite, CrystEngComm 13 (5) (Mar. 2011) 1322–1327, https://doi.org/10.1039/c0ce00533a.
[65] C. Li, B. Liang, S.P. Chen, Combined milling-dissolution of Panzhihua ilmenite in sulfuric acid, Hydrometallurgy 82 (1–2) (Jul. 2006) 93–99, https://doi.org/10.1016/j.hydromet.2006.04.001.
[66] T. Tao, L. He, J. Li, Y. Zhang, Large scale synthesis of TiO2-carbon nanocomposites using cheap raw materials as anode for lithium ion batteries, J. Alloys Compd. 615 (Dec. 2014) 1052–1055, https://doi.org/10.1016/j.jallcom.2014.07.167.
[67] L. Zhang, H. Hu, L. Wei, Q. Chen, J. Tan, Hydrochloric acid leaching behaviour of mechanically activated Panxi ilmenite (FeTiO 3), Separ. Purif. Technol. 73 (2) (Jun. 2010) 173–178, https://doi.org/10.1016/j.seppur.2010.03.022.
[68] F. Wu, et al., Hydrogen peroxide leaching of hydrolyzed titania residue prepared from mechanically activated Panzhihua ilmenite leached by hydrochloric acid, Int. J. Miner. Process. 98 (1–2) (Jan. 2011) 106–112, https://doi.org/10.1016/j.minpro.2010.10.013.
[69] P. Tan, H.P. Hu, L. Zhang, Effects of mechanical activation and oxidation-reduction on hydrochloric acid leaching of Panxi ilmenite concentration, Trans. Nonferrous Met. Soc. China (English Ed. 21 (6) (Jun. 2011) 1414–1421, https://doi.org/10.1016/S1003-6326(11)60875-3.
[70] B.N. Akhgar, M. Pazouki, M. Ranjbar, A. Hosseinnia, M. Keyanpour-Rad, Preparation of nanosized synthetic rutile from ilmenite concentrate, Miner. Eng. 23 (7) (Jun. 2010) 587–589, https://doi.org/10.1016/j.mineng.2010.01.007.
[71] B.N. Akhgar, M. Pazouki, M. Ranjbar, A. Hosseinnia, R. Salarian, Application of Taguchi method for optimization of synthetic rutile nano powder preparation from ilmenite concentrate, Chem. Eng. Res. Des. 90 (2) (Feb. 2012) 220–228, https://doi.org/10.1016/j.cherd.2011.07.008.
[72] Y. Chen, J.S. Williams, S.J. Campbell, G.M. Wang, Increased dissolution of ilmenite induced by high-energy ball milling, Mater. Sci. Eng., A 271 (1–2) (Nov. 1999) 485–490, https://doi.org/10.1016/s0921-5093(99)00441-4.
[73] N.J. Welham, D.J. Llewellyn, Mechanical enhancement of the dissolution of ilmenite, Miner. Eng. 11 (9) (Sep. 1998) 827–841, https://doi.org/10.1016/S0892-6875(98)00070-3.
[74] C. Li, B. Liang, L. hong Guo, Z. bin Wu, Effect of mechanical activation on the dissolution of Panzhihua ilmenite, Miner. Eng. 19 (14) (Nov. 2006) 1430–1438, https://doi.org/10.1016/j.mineng.2006.02.005.
[75] P. Baláž, Mechanical activation in hydrometallurgy, Int. J. Miner. Process. 72 (1–4) (Sep. 2003) 341–354, https://doi.org/10.1016/S0301-7516(03)00109-1.
[76] C. Li, B. Liang, X. Liang, Leaching kinetics of mechanically activated ilmenite ore [J],, J. Sichuan Univ. (Engineering Sci. Ed. 1 (2005).
[77] B. Liang, C. Li, C. Zhang, Y. Zhang, Leaching kinetics of Panzhihua ilmenite in sulfuric acid, Hydrometallurgy 76 (3–4) (Mar. 2005) 173–179, https://doi.org/10.1016/j.hydromet.2004.10.006.
[78] X.S.H. Zhuoshu, The kinetics of panzhihua ilmenite leaching with sulfuric acid, Min. Metall. Eng. 1 (1993).
[79] A.F.M. Barton, S.R. McConnel, Rotating disc dissolution rates of ionic solids. Part 3. - natural and synthetic ilmenite, J. Chem. Soc. Faraday Trans. 1 Phys. Chem. Condens. Phases 75 (Jan. 1979) 971–983, https://doi.org/10.1039/F19797500971, 0.
[80] C. Sasikumar, D.S. Rao, S. Srikanth, B. Ravikumar, N.K. Mukhopadhyay, S.P. Mehrotra, Effect of mechanical activation on the kinetics of sulfuric acid leaching of beach sand ilmenite from Orissa, India, Hydrometallurgy 75 (1–4) (Nov. 2004) 189–204, https://doi.org/10.1016/j.hydromet.2004.08.001.
[81] P. Baláž, Influence of solid state properties on ferric chloride leaching of mechanically activated galena, Hydrometallurgy 40 (3) (Mar. 1996) 359–368, https://doi.org/10.1016/0304-386X(95)00011-5.
[82] K. Tkáčová, P. Baláž, B. Mišura, V.E. Vigdergauz, V.A. Chanturiya, Selective leaching of zinc from mechanically activated complex CuPbZn concentrate, Hydrometallurgy 33 (3) (Jul. 1993) 291–300, https://doi.org/10.1016/0304-386X(93)90068-O.
[83] N.J. Welham, Enhanced dissolution of tantalite/columbite following milling, Int. J. Miner. Process. 61 (3) (Mar. 2001) 145–154, https://doi.org/10.1016/S0301-7516(00)00032-6.
[84] P.(Peter, Baláž, Extractive Metallurgy of Activated Minerals, Elsevier Science B.V, 2000.
[85] C. Sasikumar, D.S. Rao, S. Srikanth, N.K. Mukhopadhyay, S.P. Mehrotra, Dissolution studies of mechanically activated Manavalakurichi ilmenite with HCl and H2SO4, Hydrometallurgy 88 (1–4) (Aug. 2007) 154–169, https://doi.org/10.1016/j.hydromet.2007.03.013.
[86] T. Tao, et al., Ilmenite FeTiO3 nanoflowers and their pseudocapacitance, J. Phys. Chem. C 115 (35) (Sep. 2011) 17297–17302, https://doi.org/10.1021/jp203345s.
[87] A.M. Amer, Alkaline pressure leaching of mechanically activated Rosetta ilmenite concentrate, Hydrometallurgy 67 (1–3) (Dec. 2002) 125–133, https://doi.org/10.1016/S0304-386X(02)00164-0.
[88] T.P.B. Rajakaruna, C.P. Udawatte, R. Chandrajith, R.M.G. Rajapakse, Nonhazardous process for extracting pure titanium dioxide nanorods from geogenic ilmenite, ACS Omega 5 (26) (Jul. 2020) 16176–16182, https://doi.org/10.1021/acsomega.0c01756.
[89] J.P. Van Dyk, N.M. Vegter, P.C. Pistorius, Kinetics of ilmenite dissolution in hydrochloric acid, Hydrometallurgy 65 (1) (Jul. 2002) 31–36, https://doi.org/10.1016/S0304-386X(02)00063-4.
[90] A.R. Gharakhlou, M.N. Sarvi, Synthesis of mesoporous nanoparticles of TiO2 from ilmenite, Mater. Res. Express 4 (2) (Feb. 2017), https://doi.org/10.1088/2053-1591/aa5bab, 025027.